Atmos. Chem. Phys. Discuss., 15, 22291–22329, 2015
www.atmos-chem-phys-discuss.net/15/22291/2015/
doi:10.5194/acpd-15-22291-2015

Atmospheric Chemistry and Physics Discussions
Open Access

Upper tropospheric water vapour variability at high latitudes – Part 1: Influence of the annular modes

C. E. Sioris[1], J. Zou[2], D. A. Plummer[3], C. D. Boone[4], C. T. McElroy[1], P. E. Sheese[2], O. Moeini[1], and P. F. Bernath[4,5]

[1]Department of Earth and Space Science and Engineering, York University, Toronto, Canada, 4700 Keele St., Toronto, ON, M3J 1P3, Canada
[2]Department of Physics, University of Toronto, 60 St. George St., Toronto, ON, M5S 1A7, Canada
[3]Canadian Centre for Climate Modelling and Analysis, Environment Canada, Victoria, BC, Canada
[4]Department of Chemistry, University of Waterloo, 200 University Ave. W, Waterloo, ON, N2L 3G1, Canada
[5]Department of Chemistry and Biochemistry, Old Dominion University, 4541 Hampton Blvd., Norfolk, 23529, VA, USA

Received: 3 July 2015 – Accepted: 4 August 2015 – Published: 20 August 2015

Correspondence to: C. E. Sioris (csioris@cfa.harvard.edu)

Published by Copernicus Publications on behalf of the European Geosciences Union.

Abstract

Seasonal and monthly zonal medians of water vapour in the upper troposphere and lower stratosphere (UTLS) are calculated for both Atmospheric Chemistry Experiment (ACE) instruments for the northern and southern high-latitude regions (60–90 and 60–90° S). Chosen for the purpose of observing high-latitude processes, the ACE orbit provides sampling of both regions in eight of 12 months of the year, with coverage in all seasons. The ACE water vapour sensors, namely MAESTRO (Measurements of Aerosol Extinction in the Stratosphere and Troposphere Retrieved by Occultation) and the Fourier Transform Spectrometer (ACE-FTS) are currently the only satellite instruments that can probe from the lower stratosphere down to the mid-troposphere to study the vertical profile of the response of UTLS water vapour to the annular modes.

The Arctic oscillation (AO), also known as the northern annular mode (NAM), explains 64 % ($r = -0.80$) of the monthly variability in water vapour at northern high-latitudes observed by ACE-MAESTRO between 5 and 7 km using only winter months (January to March 2004–2013). Using a seasonal timestep and all seasons, 45 % of the variability is explained by the AO at 6.5 ± 0.5 km, similar to the 46 % value obtained for southern high latitudes at 7.5 ± 0.5 km explained by the Antarctic oscillation or southern annular mode (SAM). A large negative AO event in March 2013 produced the largest relative water vapour anomaly at 5.5 km (+70 %) over the ACE record. A similarly large event in the 2010 boreal winter, which was the largest negative AO event in the record (1950–2015), led to >50 % increases in water vapour observed by MAESTRO and ACE-FTS at 7.5 km.

1 Introduction

Water vapour is the most important greenhouse gas in the atmosphere (Lacis et al., 2010) playing an important role in climate change by magnifying changes in radiative forcing by longer-lived greenhouse gases through the water vapour feedback (Dessler

ACPD
15, 22291–22329, 2015

Upper tropospheric water vapour variability at high latitudes – Part 1

C. E. Sioris et al.

and Sherwood, 2009). A variety of observations have shown that, at near-global scales, specific humidity in the troposphere has been increasing along with atmospheric temperatures in a manner consistent with that predicted by the Clausius–Clapeyron equation – approximately 7 % K^{-1} (Hartmann et al., 2013). Long-term increases in water vapour are expected in the troposphere due to long-term increases in temperature and the resulting exponential increase in saturation vapour pressure (Soden and Held, 2006). In the middle stratosphere, long-term changes in water vapour may result from changes in the temperature of the tropical tropopause "coldpoint" that controls the dehydration of tropospheric air as it enters the stratosphere (Brewer, 1949) and from changes in its stratospheric source gas, namely methane (Oman et al., 2008). Water vapour in the extratropical lowermost stratosphere may be additionally influenced by changes in isentropic transport from the subtropics (Dessler et al., 2013). Additionally, absorption by atmospheric water vapour of radiation at terahertz and radio frequencies is a serious impediment for radio astronomy and for long-distance communications (Suen et al., 2014). The vertical distribution of water vapour is relevant for all of the effects mentioned.

In order to understand and attribute long term changes, internal modes of variability, particularly those with longer periods, should be considered simultaneously. In the extratropics, the annular modes explain more of the month-to-month and year-to-year variance of the atmospheric flow than any other climatic phenomenon (Thompson and Wallace, 2000; http://www.atmos.colostate.edu/ao/introduction.html). The northern and southern annular modes (NAM, SAM), also known as the Arctic oscillation (AO) and Antarctic oscillation (AAO) respectively, produce a strong zonal flow at mid-latitudes during their positive phase with an equatorward meridional flow near 60° latitude and weaker zonal flow accompanied by an increased tendency for poleward flow during the negative phase (Thompson and Wallace, 2000). In the high-latitude upper troposphere, where water vapour enhancements due to evaporation at the surface are minor relative to the lower troposphere, it is the negative phase of the annular modes that is expected to increase water vapour by increased transport from more

ACPD
15, 22291–22329, 2015

humid lower latitudes. Devasthale et al. (2012) used the Atmospheric Infrared Sounder (AIRS) on the Aqua satellite to study the longitudinal and vertical structure of water vapour in the 67–82° N band and interpreted the observed structure by separating the observations according to the phases of the Arctic oscillation. To our knowledge, no one has studied the impact of the Antarctic oscillation on upper tropospheric water vapour (UTWV).

The AO exhibits the largest variability during the cold season (Thompson and Wallace, 2000). Groves and Francis (2002) related TOVS (TIROS Operational Vertical Sounder) precipitable water vapour net fluxes across 70° N in winter to the phase of the AO. Li et al. (2014) showed that the longwave radiative forcing anomaly due to NAM-related variability of cold season water vapour for the 2006 to 2011 period is small ($\sim -0.2\,\mathrm{W\,m^{-2}}$).

Here, the relationship between water vapour in the upper troposphere and lower stratosphere (UTLS) at northern and southern high-latitudes (60–90 and 60–90° N) and their respective annular modes is studied using observations from satellite-based limb profilers. A particular focus is the height dependence of the relationship: does it extend up to or above the tropopause?

2 Method

2.1 Satellite observations

SCISAT was launched in 2003 carrying a suite of solar occultation instruments to carry out the mission named the Atmospheric Chemistry Experiment (ACE) (Bernath et al., 2005). The ACE instruments measuring water vapour are Measurements of Aerosol Extinction in the Stratosphere and Troposphere Retrieved by Occultation (MAESTRO) (McElroy et al., 2007) and the Fourier Transform Spectrometer (FTS) (Bernath et al., 2005). The ACE datasets begin in February 2004. The measurements provide a unique combination of high vertical resolution and the ability to measure the water vapour pro-

ACPD
15, 22291–22329, 2015

file from the mid-troposphere to the lower stratosphere where the volume mixing ratio (VMR) is < 10 ppm (parts per million), below the lower detection limit of the nadir-sounding AIRS (Gettelman et al., 2004). HIRS (High-Resolution Infrared Radiation Sounder) is the nadir sounder used in the last two Intergovernmental Panel on Climate Change (IPCC) assessments (e.g. Hartmann et al., 2013) for long-term trend studies of upper tropospheric humidity (Soden et al., 2005; Shi and Bates, 2011). However, the trend analysis of the HIRS dataset is confined to the region 60° N to 60° S because the atmosphere is much more transparent in the polar regions and the ice sheets of Greenland and Antarctica are elevated, leading to a surface contribution that complicates the application of the radiance-to-humidity relationship at high latitudes (Bates and Jackson, 2001). The Tropospheric Emission Spectrometer (TES) should also be mentioned, but in polar regions at pressures < 400 mb, the vertical resolution of TES is 11.6 km and the number of degrees of freedom of signal is < 1 (Worden et al., 2004). IASI (Infrared Atmospheric Sounding Interferometer) (Herbin et al., 2009) shows sensitivity to water vapour in polar regions up to 10 km but with a 6 km vertical resolution at this upper altitude limit. Similarly, Wiegele et al. (2014) show that IASI can retrieve water vapour profiles at Kiruna (68°) up to ∼ 8 km with ∼ 4 km vertical resolution. Other current limb sounders include the sub-millimetre radiometer on Odin which can only measure in the upper troposphere in the tropics (Rydberg et al., 2009) and the Microwave Limb Sounder on Aura which can only probe down to 316 mb (∼ 8 km) (Su et al., 2006). The fact that MAESTRO and ACE-FTS are on the same platform is extremely valuable for comparing the month-to-month variations of atmospheric constituents observed by both instruments.

MAESTRO measures absorption of solar radiation by water vapour in the ∼ 940 nm overtone-combination band (Sioris et al., 2010). The water vapour retrieval method follows the one used previously (Sioris et al., 2010). Some of the main changes are described here. The maximum allowable optical depth in the water vapour fitting window (926.0–969.7 nm) is reduced from 7.63 to 6.7. This reduces the number of noisy spectra but also possibly increases susceptibility to a dry bias at the lowest altitudes where the apparent water vapour optical depth (i.e. at MAESTRO spectral resolution) can be 4 to 5 at ~ 935 nm, the wavelength of maximum absorption. Also, MODTRAN 5.2 is now used for forward modelling and relies on the HITRAN 2008 spectroscopic database (Rothman et al., 2009). The water vapour absorption line intensities are mostly from Brown et al. (2002) and have uncertainties of 2–5 %, an improvement relative to Sioris et al. (2010) which used MODTRAN 4 (relying on HITRAN 1996). Water vapour profiles are retrieved from all available MAESTRO optical depth spectra (version 3.12, spanning 2004 to 2013) from the ongoing ACE mission. For version 3.12 optical depth spectra, the tangent height registration relies on matching simulated O_2 slant columns obtained from air density profiles, based on temperature and pressure retrieved from ACE-FTS (Boone et al., 2013), with slant columns observed by MAESTRO using the O_2 A band. The water vapour profiles are retrieved on an altitude grid that matches the vertical sampling, typically 0.4–0.6 km in the upper troposphere. MAESTRO water vapour mixing ratios that are more than twice as large as all other mixing ratios at any altitude in the same month were examined in detail and filtered if related to a measurement problem. Significant outliers are not numerous and no recursion is necessary. No other filtering is necessary. ACE-FTS gridded version 3.5 data are used in the study. The FTS retrieval is described by Boone et al. (2013). ACE-FTS water vapour with retrieval uncertainty of > 100 % are filtered as well as data points that are significantly negative (i.e. magnitude of mixing ratio is greater than retrieval uncertainty). Polar Ozone and Aerosol Measurement III (POAM III) water vapour measurements are also used to compare the observed seasonal cycle. Only version 4 data (Lumpe et al., 2006) with a flag of 0 are used.

2.2 Retrieval uncertainties and validation

POAM III has been validated down to 8 km or ~ 300 mb (Nedoluha et al., 2002; Lumpe et al., 2006) and this is used as the POAM III lower altitude limit in this work. Previous comparisons between MAESTRO and ACE-FTS have been favourable (Sioris et al., 2010; Carleer et al., 2008). ACE-FTS water vapour has been used in the val-

ACPD
15, 22291–22329, 2015

idation of other instruments (e.g. Lambert et al., 2007) and in the Stratospheric Processes And their Role in Climate (SPARC) Data Initiative (Hegglin et al., 2013). Waymark et al. (2013) compared version 3 ACE-FTS water vapour data with the previous well-validated version 2.2 (e.g. Carleer et al., 2008) and found 2 % differences over a large altitude range. Since the MAESTRO tangent height registration has improved substantially since the previous publication (Sioris et al., 2010), the current version of MAESTRO water vapour profiles has been validated in a global sense vs. ACE-FTS in the companion paper.

Beside the validation results, it is also valuable to look at retrieval uncertainties to understand the expected data quality. Based on an analysis of one year of southern high-latitude data, the MAESTRO water vapour retrieval relative uncertainty is found to be best at the lowest retrieval altitude of 5 km and is typically $\sim 30\,\%$ for a 0.4 km thick layer. The smallest retrieval relative uncertainty of 2 % for ACE-FTS occurs typically at 8.5 km (considering 5.5 to 19.5 km) and rapidly deteriorates below 7 km to 15 % based on northern high-latitude data (2004–2013) on a 1 km altitude grid.

2.3 Tropopause definitions

For the Northern Hemisphere, the monthly tropopause height is defined by the lower of the thermal tropopause or the lowest height at which the lapse rate is $< 2\,\mathrm{K\,km^{-1}}$ in monthly median temperatures from the Global Environmental Multiscale (GEM) regional assimilation system (Laroche et al., 1999). In the Southern Hemisphere, due to the extreme cold in the winter lower stratosphere, the tropopause is defined as the lower of the thermal tropopause or the lowest height at which the lapse rate is $2\,\mathrm{K\,km^{-1}}$ in monthly maximum temperatures from the GEM assimilation system. The lapse rate tropopause concept has been used previously for the extratropics (e.g. Randel et al., 2012). With this definition, the climatological tropopause at southern high latitudes is at 10.5 km for the winter half of the year (May–October) and at 9.5 km in the summer half (November to April).

ACPD
15, 22291–22329, 2015

2.4 Anomalies

To arrive at water vapour anomalies, there are three steps: creation of the time series (e.g. monthly or seasonal), compilation of the climatology, and deseasonalization. To create monthly medians for northern high latitudes, occultation profiles in the 60–90° N latitude band are selected. At southern high latitudes (60–90° S), monthly means are preferred particularly for MAESTRO instead of medians to avoid a low bias in the widely dehydrated winter lower stratosphere. The sampling provided by the ACE orbit as a function of latitude and month is illustrated by Randel et al. (2012). The consequence of the non-uniform latitudinal sampling as a function of month for the purpose of this study is discussed in Sect. 2.5. This sampling pattern repeats annually. Because ACE instruments sample southern high latitudes in only eight of twelve calendar months, November, January, March–May and July–September represent spring, summer, autumn and winter, respectively, when a seasonal timescale is used. In the north, climatological values are obtained for all calendar months except April, June, August, and December. The seasonal anomalies use the following groupings: winter consists of January and February, spring includes March and May, summer is composed of July and September and the fall is represented by October and November.

Vertically, the binning is done in 1.0 km intervals centered between 5.5 and 22.5 km (above 23 km, the MAESTRO water vapour absorption signal tends to be below the lower detection limit). The monthly mean at a given altitude bin is included in the climatology and anomaly dataset if there are ≥ 20 observations per month. A single MAESTRO profile can supply more than one observation per altitude bin since the water vapour retrieval is done on the tangent height (TH) grid, which is as fine as 0.4 km at the lowest TH of 5 km and as the angle widens between line-of-sight and the orbital track. The same process is followed with ACE-FTS and POAM III data to generate monthly median and mean time series.

The monthly climatology, used to deseasonalize the time series, is generated by averaging the monthly medians and means over the available years. Figure 1 illustrates

ACPD
15, 22291–22329, 2015

the bias between MAESTRO and ACE-FTS water vapour climatologies at both high latitude bands. An ACE-FTS high bias of ~ 10 % has been observed for the extratropical upper troposphere (40–80° N and 40–80° S, near 300 hPa) (Hegglin et al., 2013). While inconclusive, a general wet bias between 5 and 8 km is also suggested by lidar comparisons in the extratropics (Carleer et al., 2008; Moss et al., 2013). Accounting for an upper tropospheric +10 % wet bias in ACE-FTS, MAESTRO and ACE-FTS agree within ±20 % at all heights (5.5–17.5 km, in 1 km steps) in both hemispheres at high latitudes.

At each height, the monthly climatology (e.g., Fig. 4) is subtracted from the time series (e.g., Fig. 3) to give the absolute deseasonalized anomaly. Dividing the monthly absolute anomaly by the monthly climatology gives the relative anomaly. Note that July and August 2011 were omitted from the MAESTRO southern high latitude climatology at 6.5–9.5 km (altitudes and months of Puyehue volcanic enhancement) since the AAO standard error determined by regression is improved in doing so (see Sect. 2.5). The same process is followed to generate anomalies of temperature, ozone, relative humidity (RH), tropopause pressure, and tropopause height. The anomalies of relative humidity with respect to ice are based on pressure and temperature from the GEM assimilation system and an accurate saturation vapour pressure formulation (Murray, 1967). The latitude sampling anomaly is generated by calculating the average sampled latitude for each high-latitude band and then the mission-averaged latitude in each high-latitude band is subtracted.

Note that, because conclusions below about the importance of the annular modes are reached based on water vapour anomalies and the fact the deseasonalization is sensor-specific (i.e. the time series observed by each instrument is deseasonalized using its own climatology), overall biases and seasonally-dependent biases are actually inconsequential. Relevant biases are discussed in Sect. 2.5.

ACPD
15, 22291–22329, 2015

2.5 Regression analysis

We use a multiple linear regression analysis to determine the contribution of the appropriate annular mode to the variability in deseasonalized water vapour at high latitudes as a function of altitude. The set of available basis functions include a linear trend, the monthly AAO (Mo, 2000) and AO (Larson et al., 2005) indices (http://www.cpc.noaa.gov/products/precip/CWlink/) and a latitude sampling anomaly time series. This basis function is included to illustrate that sampling biases are minor even on a monthly time scale (using only the eight months which sample each high-latitude region). Note that the AO index is calculated following the method of Thompson and Wallace (2000).

When determining the response of water vapour to the AO, the AO index plus a constant are used, and the linear trend is included if it is significant at the 1σ level. When examining trend uncertainty reduction (Sect. 4.1), the regression uses a linear trend, plus a constant; the annular mode index term is included for trend determination if it improves the trend uncertainty without biasing the trend at the 1σ level.

The types of biases that could affect the analysis of water vapour variability are due to:

1. latitudinal sampling non-uniformity (Toohey et al., 2013),

2. interannual biases.

Regarding the non-uniform sampling of latitudes by the ACE orbit discussed in Sect. 2.1, the correlation between monthly time series of average sampled latitude in the northern high-latitude region and the Arctic oscillation index is 0.19 and similarly the correlation between the monthly time series of average sampled latitude in the southern high-latitude region and the Antarctic oscillation index is 0.12. Given these very low correlations, ACE's latitudinal sampling should have a negligible impact on any conclusion about the response of the observed water vapour anomaly to the annular modes, although this is tested using the latitude sampling anomaly as a basis func-

ACPD
15, 22291–22329, 2015

tion. Toohey et al. (2013) estimated monthly mean sampling biases in the UTLS to be ≤ 10 % for the category of instruments that includes ACE-FTS (and MAESTRO). The interannual biases are also < 10 % given that Sect. 3.2 below shows that approximately half of the southern high-latitude water vapour seasonal anomaly (typically ±10 % in amplitude) can be explained by interannual variability in the Antarctic oscillation (i.e. real dynamical variability, not artificial instrument-related variability). Also, there are no known issues with either MAESTRO or ACE-FTS specific to a certain year. Furthermore, the self-calibrating nature of solar occultation, combined with the wavelength stability of spectrometers (relative to filter photometers) minimize interannual bias for MAESTRO and ACE-FTS. For example, any variation in the optical (or quantum) efficiency of the instrument does not need to be calibrated as it does with an instrument measuring nadir radiance.

3 Results

The MAESTRO water vapour record (Fig. 2) at southern high latitudes is similar to the records of contemporary limb sounders as shown in Fig. 13 of Hegglin et al. (2013). The southern high-latitude time series has slightly less water in the UTLS in late winter than at northern high-latitudes (Fig. 3) due to the colder air temperatures.

3.1 Seasonal cycle

The dehydration in September that extends downward into the upper troposphere at southern high-latitudes (Fig. 4) is clearly observed by MAESTRO annually (Fig. 2). In the upper troposphere, the September dehydration is a cumulative effect of local condensation (see also Randel et al., 2012) with the temperatures at 9.5 km reaching so low that the corresponding saturation mixing ratio can be as low as 4.4 ppm, much lower than minimum mixing ratios observed in the troposphere outside the Antarctic. In

ACPD
15, 22291–22329, 2015

the mid-troposphere, the driest month shifts closer to mid-winter (e.g. August). This is observed by both ACE instruments and by POAM III.

The vertical distribution of the lower stratospheric dehydration resembles that measured from other solar occultation instruments: HALOE (Halogen Occultation Experiment) and POAM III in that the lowest water vapour mixing ratios occur at pressures higher than 100 hPa (below 16 km) (Hegglin et al., 2013). The MAESTRO climatological mean mixing ratio for September exhibits a minimum at 12.5 km altitude with a value of 2.9 ppm (Fig. 4), which compares well with the September minimum values observed by other instruments (Hegglin et al., 2013). Also, the stratospheric monthly medians are reasonable with mixing ratios < 7.5 ppm up to 22.5 km, the upper altitude limit of the climatology.

The variability in the UTWV at southern high latitudes on a monthly timescale is dominated by the seasonal cycle. The observed seasonal variation is a factor of ~ 5 at 8.5 km (Fig. 5). The seasonal cycle in water vapour is consistent with the ratio of maximum to minimum saturation vapour mixing ratio at 8.5 km of 4.6 ($\pm 1\sigma$ range: 3.9–5.3), obtained for a typical year, namely 2010, using analysis temperatures and pressures from the GEM assimilation system, sampled at ACE measurement locations for January and August, the months corresponding to the maximum and minimum water vapour in ACE-FTS and POAM III data at 8.5 km. This is in stark contrast to weak (30 %) seasonal variations in lower stratospheric (13.5 km) monthly means, according to MAESTRO observations. The large seasonal cycle amplitude in saturation vapour mixing ratio in the lower stratosphere is largely due to the extremely cold temperatures in September.

The stronger seasonal cycle at northern high-latitudes (e.g. at 5.5 km) is partly due to the non-uniform latitudinal sampling differences in the months of maximum and minimum water vapour VMR, particularly in the Southern Hemisphere. The Northern Hemisphere seasonal cycle amplitude vertical profile (Fig. 6) is thus a truer reflection of the amplitude of the seasonal cycle at $\sim 70^\circ$ N. Figures 5 and 6 illustrate that the seasonal cycle amplitude of observed water vapour VMR in the lower stratosphere departs from

ACPD
15, 22291–22329, 2015

the seasonal cycle amplitude of the saturated VMR due to the isolation of this overlying atmospheric region from large sources of water vapour. Sioris et al. (2010) studied the seasonal cycle in the 60–70° N band using an earlier version of the MAESTRO dataset. They incorrectly concluded that saturation vapour pressure changes could not explain the seasonal cycle assuming the seasonal cycle amplitude in temperature at 8.5 km was only 8 K (based on climatological subarctic winter and summer temperature profiles). According to GEM temperature analyses, the seasonal cycle amplitude is 18 K with a sharp peak in mid-summer (e.g. July) and generally sufficient to explain the seasonal variation and its vertical dependence in the upper troposphere (Fig. 6).

In spite of the large tropospheric seasonality at high latitudes, it is possible to deseasonalize the water vapour records from the ACE instruments and investigate the remaining sources of temporal variability, as shown next.

3.2 Antarctic oscillation

At 8.5 km, where the largest anti-correlations exist between MAESTRO water vapour at 8.5 km and the AAO index, it is observed that the anti-correlation is stronger on a seasonal timescale ($R = -0.53$) rather than a monthly timescale. Stronger anti-correlation ($R = -0.68$) at the seasonal timescale is also found for ACE-FTS water vapour at 7.5 ± 0.5 km, the altitude of its strongest anti-correlation with the AAO index. Thus, in Fig. 7, the MAESTRO and ACE-FTS seasonal median relative anomaly for 8.5 ± 0.5 and 7.5 ± 0.5 km, respectively, are presented. The use of medians is preferable for detecting the AAO response in the troposphere where the water vapour mixing ratios are not normally distributed. The monthly medians are also less susceptible to outliers in the individual retrieved profiles. The large positive anomaly in 2011 is due to the most explosive eruption of a volcano in the last 24 years, namely Puyehue, and will be discussed in the forthcoming companion paper.

At 8.5 km, where the response of water vapour to AAO has the smallest relative uncertainty for both ACE-FTS and MAESTRO, the response ranges between +23 and −18 % for individual seasons and the standard deviation of the AAO response is 10 %

ACPD
15, 22291–22329, 2015

(2004–2012). The anomalies in the upper troposphere are highly correlated with each other (e.g. $R = 0.79$ for MAESTRO absolute anomalies at 8.5 vs. 9.5 km on a monthly timescale). In the stratosphere (altitude ≥ 10 km), the response of MAESTRO water vapour to AAO is weak (not significant). Figure 8 illustrates the vertical profile of the AAO response. There is a strong vertical correlation between the water vapour responses to the AAO observed by the two instruments and the responses are statistically significant (up to the 4σ level for ACE-FTS at 7.5 km) in the 5.5–8.5 km for both instruments indicating that the AAO affects water vapour throughout the upper troposphere at southern high latitudes. The MAESTRO and ACE-FTS AAO fitting coefficients are not different from 0 at the 1σ level at 10.5 and 11.5 km, respectively. Slight differences between the ACE instruments may relate to differences in their respective fields of view (FOV). MAESTRO's FOV is 1 km in the vertical direction, whereas ACE-FTS, because of its 3.7 km circular field of view at a tangent point 10 km above the ground, will see some contribution from the troposphere even when the FOV is centered 1.5 km above the tropopause. Given that the ACE-FTS field of view is circular, the full-width at half-maximum of the FOV is 3.2 km. Due to vertical oversampling of the FOV, the vertical resolution of the water vapour products from each ACE instrument is finer than the height of the FOV (see also Sioris et al., 2010). Nevertheless, differences in vertical resolution between the ACE instruments will lead to a slight difference in terms of the peak altitude of the anti-correlation between the water vapour anomaly and AAO. The impact of non-uniform latitudinal sampling is discussed in Sect. 3.3.

As stated in Sect. 1, the AO is most active in the winter when the surface is coldest. Therefore less infrared (IR) radiation is emitted and trapped by AO-related increases in atmospheric water vapour. Over Antarctica, the AAO instead shows strength in late spring (Thompson and Wallace, 2000) at a time when there is increased IR radiation emitted by the surface, possibly making AAO-related water vapour changes more likely to lead to increases in temperature at the surface and to reduce outgoing longwave flux at the top of the atmosphere (TOA). The impact of AAO-induced variability of upper tropospheric water vapour on surface climate and outgoing longwave flux at the top of the atmosphere is assessed for November 2009 and November 2010, two months when the AAO was of opposite phase (see Appendix for details of the method). The cooling rate differences at the surface between these negative and positive phases of the AAO are trivial (< 0.07 K) in late spring (November). The outgoing longwave flux is reduced by 0.7 $\mathrm{W\,m^{-2}}$ in November 2009 relative to November 2010 due solely to AAO-related upper tropospheric changes in water vapour. Scaling this change to the typical AAO fluctuation in all seasons (1979–2014), variations of 0.2 $\mathrm{W\,m^{-2}}$ in the outgoing longwave flux at the TOA are found, which are equal to the magnitude Li et al. (2014) found for the AO-related IR flux changes at TOA due to water vapour for the Arctic cold season. Note that Li et al. (2014) found the AO-related water vapour changes to be much smaller than AO-related cloud changes.

3.3 Arctic oscillation

Figure 9 shows the altitude dependence of observed water vapour response to the Arctic oscillation using all eight months that sample the northern high-latitude region. There is a coherent and statistically significant response (up to the 4σ level for MAESTRO) to the AO observed by both instruments, with a general decrease through the upper troposphere and a vanishing response in the vicinity of the tropopause. Above 12 km, the response to the AO is insignificant at the 1σ level. The magnitude of the response to the AO is also similar to the magnitude of the response of UTWV at southern high latitudes to the Antarctic oscillation.

The spatiotemporal sampling of ACE (Bernath et al., 2005) is quite non-uniform on monthly time scales whereas on seasonal timescales the spatial coverage of the entire high-latitude region becomes more complete. This likely partly explains why a larger anti-correlation between southern high-latitude UTWV and the AAO index is found when a seasonal timestep is used. When the latitudinal sampling anomaly is used as a basis function, it is generally not a significant term in either hemisphere. Figure 9 shows that the inclusion of this term does not change the response to the AO, reinforcing the same finding for the response to the AAO (Fig. 8). Clearly, water vapour at high-latitudes is responding with high fidelity to the local annular mode.

Using the MAESTRO water vapour anomalies, a seasonal timestep and all seasons, 45 % of the variability is explained at 6.5 ± 0.5 km, similar to the fraction obtained for southern high latitudes.

It is well known that the "active season" for the AO is winter (Thompson and Wallace, 2000). Figure 10 shows a water vapour anomaly time series for an altitude of 6.5 km, composed only of January, February and March (2004–2013). The wintertime anti-correlation between the ACE-FTS water vapour anomaly and the AO index peaks at 6.5 km with $R = -0.57$. MAESTRO shows a much stronger anti-correlation of $R = -0.80$ at 6.5 and 5.5 km. A large negative AO event in March 2013 produced the largest relative water vapour anomaly at 5.5 km (+70 %) over the MAESTRO record. March 2013 was not available below 8 km for ACE-FTS but at 8.5 and 9.5 km, ACE-FTS and MAESTRO both show the largest positive anomalies for any March in either northern high-latitude data record (+32 and +35 % at 8.5 km and +16 and +27 % at 9.5 km for MAESTRO and ACE-FTS, respectively) and a vanishing enhancement at 10.5 km (above the monthly mean tropopause). A similarly large event in winter 2010, which was the largest negative AO event in the record (1950–2015), led to > 50 and 30 % increases in northern high-latitude water vapour observed at 7.5 km in January and February 2010, respectively, with agreement between MAESTRO and ACE-FTS. January 2010 has the largest anomaly at 7.5 km in any month (considering all seasons) of the northern high-latitude data records of MAESTRO and ACE-FTS. Steinbrecht et al. (2011) used a multiple linear regression analysis to demonstrate a significant increase in total column ozone (+8 Dobson units) in the winter of 2010 that was attributed to the same historically strong negative phase of the Arctic oscillation.

ACPD
15, 22291–22329, 2015

4 Discussion and conclusions

Polar regions have a strong seasonal cycle in UTWV, driven by the seasonality of the local temperature. In the Arctic upper troposphere, condensation and precipitation play a minor role in governing the water vapour abundance on monthly timescales. Near the Arctic tropopause (250–350 mb), cloud fractions are < 35 % (Treffeisen et al., 2007) and MAESTRO monthly median relative humidity at 9.5 km is < 70 % in all 63 months in which this instrument has observed the northern high-latitude region. However, dynamical variability via the annular modes has been shown here to strongly affect UTWV at high latitudes. Apart from the seasonal cycle, the Antarctic oscillation is a dominant mode of variability in upper tropospheric (∼ 8 km) water vapour at southern high latitudes on a seasonal timescale and the Arctic oscillation explains most of the variability at wintertime UTWV in northern high latitudes.

4.1 Impact of fitting annular mode indices on decadal trends

In the most recent IPCC report, Hartmann et al. (2013) review the literature on trends in upper tropospheric water vapour observed from satellite instruments. Only one such publication is cited, namely Shi and Bates (2011). This work uses HIRS data between 85° N and 85° S, but only trends at low latitudes (30° N–30° S) are discussed. While long-term trends in polar UTWV require continued measurements and investigation, including the AO index in the trend analysis improves trend uncertainties below 12 km over the MAESTRO record (e.g. by 16 % at 6.5 km) and reduces a statistically insignificant (1σ) but consistent, positive bias in the decadal trend (2004–2013) that is found when the AO is excluded from the regression model. This bias stems from the two large negative events in the winters of 2010 and 2013 which lie near the end of the data record. The trend uncertainty reduction is 22 % upon inclusion of the Antarctic Oscillation Index into regression modelling of the linear trend in water vapour at 8.5 km at southern high-latitudes, again with no significant impact on the linear trend itself.

ACPD
15, 22291–22329, 2015

4.2 Proposed mechanisms

The amplitude of the response by water vapour to annular mode oscillations does not change significantly (1σ) whether upper tropospheric water vapour is binned vs. altitude or geopotential altitude in either hemisphere at high latitudes, indicating the insensitivity to the choice of vertical coordinate. This is important to note as the correlation of other variables with the annular modes is explored in this section.

There is some observational evidence for two mechanisms that could explain how UTWV at high latitudes responds to the annular modes. The first is through annular-mode-related air temperature fluctuations, which impact UTWV by changing the saturation mixing ratio. For changes in saturation mixing ratio to have an impact, there needs to be an available supply of upper tropospheric water vapour. The second mechanism is through changes to the meridional flux itself (e.g. Devasthale et al., 2012; Thompson and Wallace, 2000), given the latitude gradient in water vapour between high and mid-latitudes at all upper tropospheric heights.

The anti-correlation of the AAO with anomalies in southern high-latitude temperature (from analyses of the GEM assimilation system) is also studied (Fig. 11). This anti-correlation is not strong ($R = -0.34$ at 5.5 km, and monotonically less correlated with increasing height through the troposphere up to 10.5 km), indicating that southern high-latitude UTWV cannot be solely attributed to AAO-related temperature fluctuations but also requires an influx of high water vapour mixing ratios from mid-latitudes via the second proposed mechanism. This argument is supported by the larger positive correlations of the AAO with ACE-FTS ozone anomalies ($R = 0.47$ at 10.5 km, Fig. 11) which indicate that the AAO generally affects the composition of the southern high-latitude upper troposphere. For tropospheric ozone, the increasing correlation with height is likely due to the fact that latitudinal gradients in the mid-troposphere are weaker than for water vapour, and thus the dominant effect is the AAO-induced meridional swinging of vertical gradients near a tropopause which tends to decrease in height toward the pole.

ACPD
15, 22291–22329, 2015

Upper tropospheric water vapour variability at high latitudes – Part 1

C. E. Sioris et al.

At northern high latitudes, the strongest correlation of the AO with temperature in the 5.5 to 19.5 km is only $R = -0.38$ (at 6.5 km) and the correlation profile is very similar in shape and magnitude to southern high latitudes (Fig. 11). Again, the anti-correlation vs. temperature is significantly weaker than between the AO and (MAESTRO) water vapour anomalies, which reach −0.56 at 6.5 km. However, the significant correlations between AAO and ozone in the tropopause region seen in Fig. 11 for southern high-latitudes are not found in the north (Fig. 12). Thus, in the north, a combination of both mechanisms is required but the temperature-related mechanism appears to be more explanatory. This is explored further by studying the anti-correlation between relative humidity (RH) anomalies and the annular modes. At northern high-latitudes, a large difference in anti-correlation with the AO exists between relative humidity and specific humidity (i.e. water vapour VMR) (Fig. 12). This implies that the temperature-related mechanism is largely responsible for the AO-related fluctuations in water vapour, with relative humidity maintained during these monthly fluctuations. However, at southern high-latitudes, the RH anomalies anti-correlate with the AAO almost as strongly as do the water vapour anomalies, particularly near the tropopause (Fig. 11). This small difference in correlation implies that the temperature-related mechanism is less explanatory at southern high latitudes and meridional flux of relative humidity can largely explain the water vapour anti-correlation with the AAO.

Thus, it appears that the major mechanism involved in the high anti-correlations of the annular mode and water vapour anomalies could differ between the two annular modes (i.e. between hemispheres). The dynamical mechanism may be more important at southern high latitudes in the upper troposphere where latitudinal gradients in water vapour and ozone (e.g. Liu et al., 2005, 2013) are likely larger than at northern high latitudes due to the isolated nature of the former region.

Also, in the Northern Hemisphere, deep convection supplies more water vapour to the upper troposphere than in the Southern Hemisphere (Sioris et al., 2010) and these differences are expected to be due to differences in the respective extratropical regions stemming from land fraction differences. This supply of humidity via deep convection

ACPD
15, 22291–22329, 2015

to the northern extratropical upper troposphere allows AO-related temperature fluctuations to effectively increase UTWV. In the southern extratropics, the water vapour supply tends to be insufficient above 8 km as is evident for from Fig. 5 which indicates that UTWV at southern high latitudes cannot match the local seasonal cycle amplitude of saturation VMR whereas Fig. 6 shows that in the northern high-latitude region, UTWV tracks saturation VMR up to 10.5 km. Similarly, Fig. 12 shows that relative humidity anomalies below 7 km are much less correlated than UTWV anomalies with the AAO, implying that the temperature-related mechanism is generally limited to the altitude range with sufficient supply of humidity. This altitude range is quite different between hemispheres, extending closer to the tropopause in the northern high-latitude region. Furthermore, the lack of response in the stratosphere, e.g. at 13.5 km (Fig. 9), clearly above the maximum monthly tropopause height of 11.5 km, is due to the ineffectiveness of both mechanisms in spite of the large responses of both temperature and the meridional flux to the annular mode (Thompson and Wallace, 2000), peaking near 100 mb ($\sim$ 16 km) for temperature, and between 200–300 mb ($\sim$ 10 km) for the meridional flux in both hemispheres. The temperature-related mechanism is ineffective in the stratosphere because temperature increases do not entail increases in water vapour in this dry region. The meridional flux mechanism becomes ineffective at 13.5 km because the latitudinal water vapour gradients in the stratosphere are much weaker than in the troposphere.

We see no evidence in either high-latitude region of a third mechanism whereby the UTWV anomalies are simply explained by annular-mode-driven tropopause variations: the correlation between tropopause height or tropopause pressure anomalies and the relevant annular mode is not significant in either high-latitude region ($-0.1 < R < 0.1$). This is not surprising given that the magnitude of correlations of temperature and water vapour with the annular modes diminish with increasing height toward the tropopause (e.g. Fig. 12).

Longer datasets and further analysis would be helpful to understand the contribution by each proposed mechanism.

ACPD
15, 22291–22329, 2015

Appendix: Cooling rate differences

Cooling rate vertical profiles are calculated using MODTRAN5.2 (e.g. Bernstein et al., 1996) assuming an Antarctic surface altitude of 2.5 km, subarctic summer temperature profile, free tropospheric aerosol extinction (visibility of 50 km) and two water vapour cases:

1. using MAESTRO climatological median water vapour between 6.5 and 9.5 km increased by the vertically-resolved water vapour response to AAO determined by multiple linear regression (with AAO and constant as the only predictors) for November 2009, when the AAO was in its negative phase (index of −1.92).

2. same as (1), except for November 2010, when AAO index was +1.52 (positive phase).

Acknowledgements. The availability of the NOAA AAO index is appreciated. The ACE mission is supported primarily by the Canadian Space Agency. POAM III data were obtained from the NASA Langley Research Center Atmospheric Science Data Center. CES acknowledges Kaley Walker (University of Toronto) for her role in including MAESTRO in the Water Vapour Assessment (WAVAS) 2, organized by SPARC (Stratosphere–Troposphere Processes and their Role in Climate). CES also acknowledges Frédéric Laliberté (Environment Canada) for his suggestion to analyze correlations of relative humidity anomalies with the annular modes and for guidance on the interpretation of those results.

References

Bates, J. J. and Jackson, D. L.: Trends in upper-tropospheric humidity, Geophys. Res. Lett., 28, 1695–1698, 2001.

Bernath, P. F., McElroy, C. T., Abrams, M. C., Boone, C. D., Butler, M., Camy-Peyret, C., Carleer, M., Clerbaux, C., Coheur, P.-F., Colin, R., DeCola, P., DeMazière, M., Drummond, J. R., Dufour, D., Evans, W. F. J., Fast, H., Fussen, D., Gilbert, K., Jennings, D. E., Llewellyn, E. J., Lowe, R. P., Mahieu, E., McConnell, J. C., McHugh, M., McLeod, S. D., Michaud, R., Midwinter, C., Nassar, R., Nichitiu, F., Nowlan, C., Rinsland, C. P., Rochon, Y. J., Rowlands, N.,

ACPD
15, 22291–22329, 2015

Semeniuk, K., Simon, P., Skelton, R., Sloan, J. J., Soucy, M.-A., Strong, K., Tremblay, P., Turnbull, D., Walker, K. A., Walkty, I., Wardle, D. A., Wehrle, V., Zander, R., and Zou, J.: Atmospheric Chemistry Experiment (ACE): mission overview, Geophys. Res. Lett., 32, L15S01, doi:10.1029/2005GL022386, 2005.
Bernstein, L. S., Berk, A., Acharya, P. K., Robertson, D. C., Anderson, G. P., Chetwynd, J. H., and Kimball, L. M.: Very narrow band model calculations of atmospheric fluxes and cooling rates, J. Atmos. Sci., 53, 2887–2904, 1996.
Boone, C. D., Walker, K. A., and Bernath, P. F.: Version 3 retrievals for the Atmospheric Chemistry Experiment Fourier Transform Spectrometer (ACE-FTS). The Atmospheric Chemistry Experiment ACE at 10: A Solar Occultation Anthology, edited by: Bernath, P. F., A. Deepak Publishing, Hampton, Virginia, 2013.
Brewer, A. W.: Evidence for a world circulation provided by the measurements of helium and water vapour distribution in the stratosphere, Q. J. Roy. Meteor. Soc., 75, 351–363, 1949.
Brown, L. R., Toth, R. A., and Dulick, M.: Empirical line parameters of $H_2^{16}O$ near 0.94 µm: positions, intensities and air-broadening coefficients, J. Mol. Spectrosc., 212, 57–82, 2002.
Carleer, M. R., Boone, C. D., Walker, K. A., Bernath, P. F., Strong, K., Sica, R. J., Randall, C. E., Vömel, H., Kar, J., Höpfner, M., Milz, M., von Clarmann, T., Kivi, R., Valverde-Canossa, J., Sioris, C. E., Izawa, M. R. M., Dupuy, E., McElroy, C. T., Drummond, J. R., Nowlan, C. R., Zou, J., Nichitiu, F., Lossow, S., Urban, J., Murtagh, D., and Dufour, D. G.: Validation of water vapour profiles from the Atmospheric Chemistry Experiment (ACE), Atmos. Chem. Phys. Discuss., 8, 4499–4559, doi:10.5194/acpd-8-4499-2008, 2008.
Dessler, A. E. and Sherwood, S. C.: A matter of humidity, Science, 323, 1020–1021, doi:10.1126/science.1171264, 2009.
Dessler, A. E., Schoeberl, M. R., Wang, T., Davis, S. M., and Rosenlof, K. H.: Stratospheric water vapor feedback, P. Natl. Acad. Sci. USA, 110, 8087–18091, 2013.
Devasthale, A., Tjernström, M., Caian, M., Thomas, M. A., Kahn, B. H., and Fetzer, E. J.: Influence of the Arctic Oscillation on the vertical distribution of clouds as observed by the A-Train constellation of satellites, Atmos. Chem. Phys., 12, 10535–10544, doi:10.5194/acp-12-10535-2012, 2012.
Gettelman, A., Weinstock, E. M., Fetzer, E. J., Irion, F. W., Eldering, A., Richard, E. C., Rosenlof, K. H., Thompson, T. L., Pittman, J. V., Webster, C. R., and Herman, R. L.: Validation of Aqua satellite data in the upper troposphere and lower stratosphere with in situ aircraft instruments, Geophys. Res. Lett., 31, L22107, doi:10.1029/2004GL020730, 2004.

ACPD
15, 22291–22329, 2015

Groves, D. G. and Francis, J. A.: Variability of the Arctic atmospheric moisture budget from TOVS satellite data, J. Geophys. Res., 107, 4785, doi:10.1029/2002JD002285, 2002.
Hartmann, D. L., Klein Tank, A. M. G., Rusticucci, M., Alexander, L. V., Brönnimann, S., Charabi, Y., Dentener, F. J., Dlugokencky, E. J., Easterling, D. R., Kaplan, A., Soden, B. J., Thorne, P. W., Wild, M., and Zhai, P. M.: Observations: atmosphere and surface. in: Climate Change 2013: The Physical Science Basis. Contribution of Working Group I to the Fifth Assessment Report of the Intergovernmental Panel on Climate Change, edited by: Stocker, T. F., Qin, D., Plattner, G.-K., Tignor, M., Allen, S. K., Boschung, J., Nauels, A., Xia, Y., Bex, V., and Midgley, P. M., Cambridge University Press, Cambridge, UK and New York, NY, USA, 2013.
Hegglin, M. I., Tegtmeier, S., Anderson, J., Froidevaux, L., Fuller, R., Funke, B., Jones, A., Lingenfelser, G., Lumpe, J., Pendlebury, D., Remsberg, E., Rozanov, A., Toohey, M., Urban, J., von Clarmann, T., Walker, K. A., Wang, R., and Weigel, K.: SPARC Data Initiative: comparison of water vapor climatologies from international satellite limb sounders, J. Geophys. Res.-Atmos., 118, 11824–11846, doi:10.1002/jgrd.50752, 2013.
Herbin, H., Hurtmans, D., Clerbaux, C., Clarisse, L., and Coheur, P.-F.: $H_2^{16}O$ and HDO measurements with IASI/MetOp, Atmos. Chem. Phys., 9, 9433–9447, doi:10.5194/acp-9-9433-2009, 2009.
Lacis, A. A., Schmidt, G. A., Rind, D., and Ruedy, R. A.: Atmospheric CO_2: principal control knob governing Earth's temperature, Science, 330, 356–359, 2010.
Lambert, A., Read, W. G., Livesey, N. J., Santee, M. L., Manney, G. L., Froidevaux, L., Wu, D. L., Schwartz, M. J., Pumphrey, H. C., Jimenez, C., Nedoluha, G. E., Cofield, R. E., Cuddy, D. T., Daffer, W. H., Drouin, B. J., Fuller, R. A., Jarnot, R. F., Knosp, B. W., Pickett, H. M., Perun, V. S., Snyder, W. V., Stek, P. C., Thurstans, R. P., Wagner, P. A., Waters, J. W., Jucks, K. W., Toon, G. C., Stachnik, R. A., Bernath, P. F., Boone, C. D., Walker, K. A., Urban, J., Murtagh, D., Elkins, J. W., and Atlas, E.: Validation of the Aura Microwave Limb Sounder middle atmosphere water vapor and nitrous oxide measurements, J. Geophys. Res., 112, D24S36, doi:10.1029/2007JD008724, 2007.
Laroche, S., Gauthier, P., St-James, J., and Morneau, J.: Implementation of a 3D variational data assimilation system at the Canadian Meteorological Centre. Part II: The regional analysis, Atmos. Ocean, 37, 281–307, 1999.

Larson, J., Zhou, Y., and Higgins, R. W.: Characteristics of landfalling tropical cyclones in the United States and Mexico: climatology and interannual variability, J. Climate, 18, 1247–1262, 2005.
Li, Y., Thompson, D. W. J., Huang, Y., and Zhang, M.: Observed linkages between the northern annular mode/North Atlantic Oscillation, cloud incidence, and cloud radiative forcing, Geophys. Res. Lett., 41, 1681–1688, doi:10.1002/2013GL059113, 2014.
Liu, G., Liu, J., Tarasick, D. W., Fioletov, V. E., Jin, J. J., Moeini, O., Liu, X., Sioris, C. E., and Osman, M.: A global tropospheric ozone climatology from trajectory-mapped ozone soundings, Atmos. Chem. Phys., 13, 10659–10675, doi:10.5194/acp-13-10659-2013, 2013.
Liu, X., Chance, K., Sioris, C. E., Spurr, R. J. D., Kurosu, T. P., Martin, R. V., and Newchurch, M. J.: Ozone profile and tropospheric ozone retrievals from the Global Ozone Monitoring Experiment: algorithm description and validation, J. Geophys. Res., 110, D20307, doi:10.1029/2005JD006240, 2005.
Lumpe, J., Bevilacqua, R., Randall, C., Nedoluha, G., Hoppel, K., Russell, J., Harvey, V. L., Schiller, C., Sen, B., Taha, G., Toon, G., and Vömel, H.: Validation of Polar Ozone and Aerosol Measurement (POAM) III version 4 stratospheric water vapor, J. Geophys. Res., 111, D11301, doi:10.1029/2005JD006763, 2006.
McElroy, C. T., Nowlan, C. R., Drummond, J. R., Bernath, P. F., Barton, D. V., Dufour, D. G., Midwinter, C., Hall, R. B., Ogyu, A., Ullberg, A., Wardle, D. I., Kar, J., Zou, J., Nichitiu, F., Boone, C. D., Walker, K. A., and Rowlands, N.: The ACE-MAESTRO instrument on SCISAT: description, performance, and preliminary results, Appl. Optics, 46, 4341–4356, 2007.
Mo, K. C.: Relationships between low-frequency variability in the Southern Hemisphere and sea surface temperature anomalies, J. Climate, 13, 3599–3610, 2000.
Moss, A., Sica, R. J., McCullough, E., Strawbridge, K., Walker, K., and Drummond, J.: Calibration and validation of water vapour lidar measurements from Eureka, Nunavut, using radiosondes and the Atmospheric Chemistry Experiment Fourier Transform Spectrometer, Atmos. Meas. Tech., 6, 741–749, doi:10.5194/amt-6-741-2013, 2013.
Murray, F. W.: On the computation of saturation vapor pressure, J. Appl. Meteorol., 6, 203–204, 1967.
Nedoluha, G. E., Bevilacqua, R. M., Hoppel, K. W., Lumpe, J. D., and Smit, H.: Polar Ozone and Aerosol Measurement III measurements of water vapor in the upper troposphere and lowermost stratosphere, J. Geophys. Res., 107, ACH 7-1–ACH 7-10, doi:10.1029/2001JD000793, 2002.

ACPD
15, 22291–22329, 2015

Oman, L., Waugh, D. W., Pawson, S., Stolarski, R. S., and Nielsen, J. E.: Understanding the changes of stratospheric water vapor in coupled chemistry–climate model simulations, J. Atmos. Sci., 65, 3278–3291, 2008.

Randel, W. J., Moyer, E., Park, M., Jensen, E., Bernath, P., Walker, K., and Boone, C.: Global variations of HDO and HDO/H_2O ratios in the upper troposphere and lower stratosphere derived from ACE-FTS satellite measurements, J. Geophys. Res., 117, D06303, doi:10.1029/2011JD016632, 2012.

Rothman, L. S., Gordon, I. E., Barbe, A., Benner, D. C., Bernath, P. F., Birk, M., Boudon, V., Brown, L. R., Campargue, A., Champion, J.-P., Chance, K., Coudert, L. H., Dana, V., Devi, V. M., Fally, S., Flaud, J.-M., Gamache, R. R., Goldman, A., Jacquemart, D., Kleiner, I., Lacome, N., Lafferty, W. J., Mandin, J.-Y., Massie, S. T., Mikhailenko, S. N., Miller, C. E., Moazzen-Ahmadi, N., Naumenko, O. V., Nikitin, A. V., Orphal, J., Perevalov, V. I., Perrin, A., Predoi-Cross, A., Rinsland, C. P., Rotger, M., Šimečková, M., Smith, M. A. H., Sung, K., Tashkun, S. A., Tennyson, J., Toth, R. A., Vandaele, A. C., Vander Auwera, J.: The HITRAN 2008 molecular spectroscopic database, J. Quant. Spectrosc. Ra., 110, 533–572, 2009.

Rydberg, B., Eriksson, P., Buehler, S. A., and Murtagh, D. P.: Non-Gaussian Bayesian retrieval of tropical upper tropospheric cloud ice and water vapour from Odin-SMR measurements, Atmos. Meas. Tech., 2, 621–637, doi:10.5194/amt-2-621-2009, 2009.

Shi, L. and Bates, J. J.: Three decades of intersatellite-calibrated High-Resolution Infrared Radiation Sounder upper tropospheric water vapor, J. Geophys. Res., 116, D04108, doi:10.1029/2010JD014847, 2011.

Sioris, C. E., Zou, J., McElroy, C. T., McLinden, C. A, and Vömel, H.: High vertical resolution water vapour profiles in the upper troposphere and lower stratosphere retrieved from MAESTRO solar occultation spectra, Adv. Space Res., 46, 642–650, 2010.

Soden, B. J. and Held, I. M.: An assessment of climate feedbacks in coupled ocean–atmosphere models, J. Climate, 19, 3354–3360, doi:10.1175/JCLI3799.1, 2006.

Soden, B. J., Jackson, D. L., Ramaswamy, V., Schwarzkopf, M. D., and Huang, X.: The radiative signature of upper tropospheric moistening, Science, 310, 841–844, 2005.

Steinbrecht, W., Köhler, U., Claude, H., Weber, M., Burrows, J. P., and van der A, R. J.: Very high ozone columns at northern mid-latitudes in 2010, Geophys. Res. Lett., 38, L06803, doi:10.1029/2010GL046634, 2011.

ACPD
15, 22291–22329, 2015

Su, H., Read, W. G., Jiang, J. H., Waters, J. W., Wu, D. L., and Fetzer, E. J.: Enhanced positive water vapor feedback associated with tropical deep convection: new evidence from Aura MLS, Geophys. Res. Lett., 33, L05709, doi:10.1029/2005GL025505, 2006.

Suen, J. Y., Fang, M. T., and Lubin, P. M.: Global distribution of water vapor and cloud cover sites for high-performance THz applications, IEEE Trans. Terahertz Sci. Technol., 4, 86–100, 2014.

Thompson, D. W. J. and Wallace, J. M.: Annular modes in the extratropical circulation. Part I: Month-to-month variability, J. Climate, 13, 1000–1016, 2000.

Toohey, M., Hegglin, M. I., Tegtmeier, S., Anderson, J., Añel, J. A., Bourassa, A., Brohede, S., Degenstein, D., Froidevaux, L., Fuller, R., Funke, B., Gille, J., Jones, A., Kasai, Y., Krüger, K., Kyrölä, E., Neu, J. L., Rozanov, A., Smith, L., Urban, J., von Clarmann, T., Walker, K. A., and Wang, R. H. J.: Characterizing sampling biases in the trace gas climatologies of the SPARC Data Initiative, J. Geophys. Res.-Atmos., 118, 11847–11862, doi:10.1002/jgrd.50874, 2013.

Treffeisen, R., Krejci, R., Ström, J., Engvall, A. C., Herber, A., and Thomason, L.: Humidity observations in the Arctic troposphere over Ny-Ålesund, Svalbard based on 15 years of radiosonde data, Atmos. Chem. Phys., 7, 2721–2732, doi:10.5194/acp-7-2721-2007, 2007.

Waymark, C., Walker, K. A., Boone, C. D., and Bernath, P. F.: ACE-FTS version 3.0 data set: validation and data processing update, Ann. Geophys., 56, ag-6339, doi:10.4401/ag-6339, 2013.

Wiegele, A., Schneider, M., Hase, F., Barthlott, S., García, O. E., Sepúlveda, E., González, Y., Blumenstock, T., Raffalski, U., Gisi, M., and Kohlhepp, R.: The MUSICA MetOp/IASI H_2O and δD products: characterisation and long-term comparison to NDACC/FTIR data, Atmos. Meas. Tech., 7, 2719–2732, doi:10.5194/amt-7-2719-2014, 2014.

Worden, J., Kulawik, S. S., Shephard, M. W., Clough, S. A., Worden, H., Bowman, K., and Goldman, A.: Predicted errors of tropospheric emission spectrometer nadir retrievals from spectral window selection, J. Geophys. Res., 109, D09308, doi:10.1029/2004JD004522, 2004.

ACPD
15, 22291–22329, 2015

Upper tropospheric water vapour variability at high latitudes – Part 1

C. E. Sioris et al.

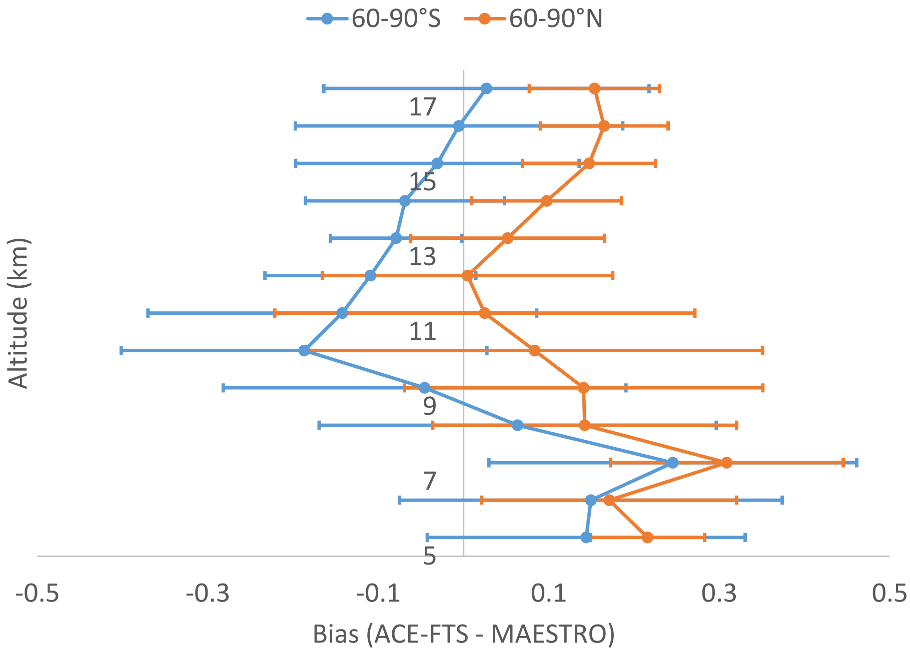

Figure 1. Orange: Relative differences between ACE-FTS and MAESTRO climatological medians averaged over the eight months sampling the northern high-latitude region and their standard deviation; blue: relative differences between ACE-FTS and MAESTRO climatological means averaged over the eight months sampling the southern high-latitude region and their standard deviation. The horizontal bars show the standard deviation of the differences between the two climatologies over the eight available months. To account for vertical resolution differences, the MAESTRO climatology was vertically smoothed with a 3 km boxcar.

ACPD
15, 22291–22329, 2015

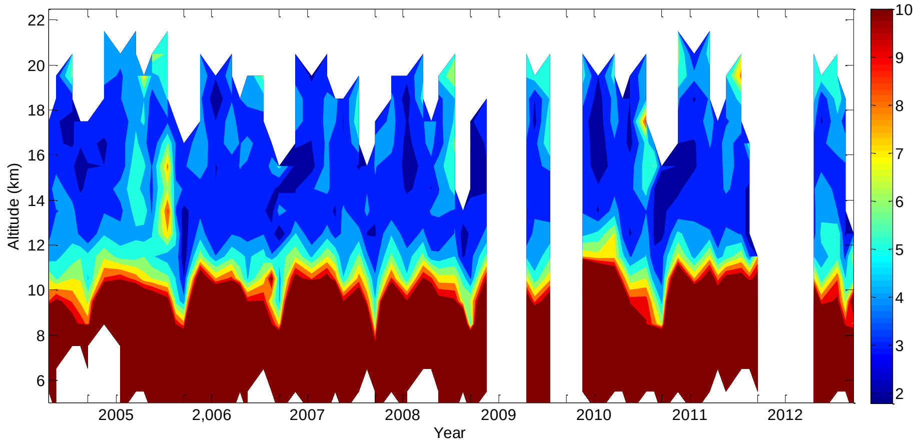

Figure 2. Time series of the MAESTRO monthly mean water vapour volume mixing ratio (VMR) vs. altitude (5.5–22.5 km) at southern high latitudes (60–90° S) with a linear colour scale (ppm), emphasizing the stratospheric variability. Unlabelled ticks along the bottom correspond to September. The time series is composed using the eight months in which ACE samples the southern high latitudes (see Sect. 2).

ACPD
15, 22291–22329, 2015

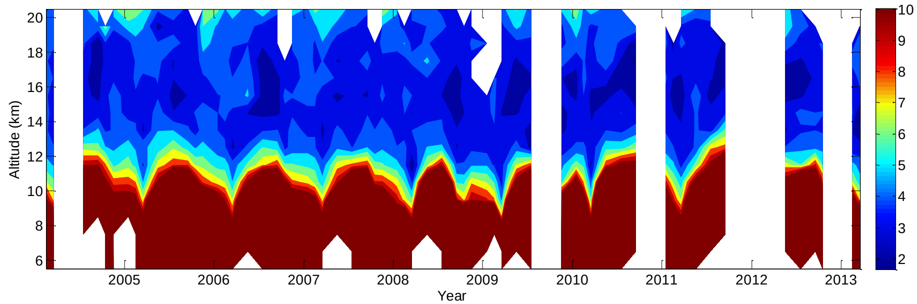

Figure 3. Time series of the MAESTRO monthly median water vapour volume mixing ratio (VMR) vs. altitude (km) at northern high latitudes (60–90° N). The time series is composed using the eight months in which ACE samples the northern high latitudes (see Sect. 2).

ACPD
15, 22291–22329, 2015

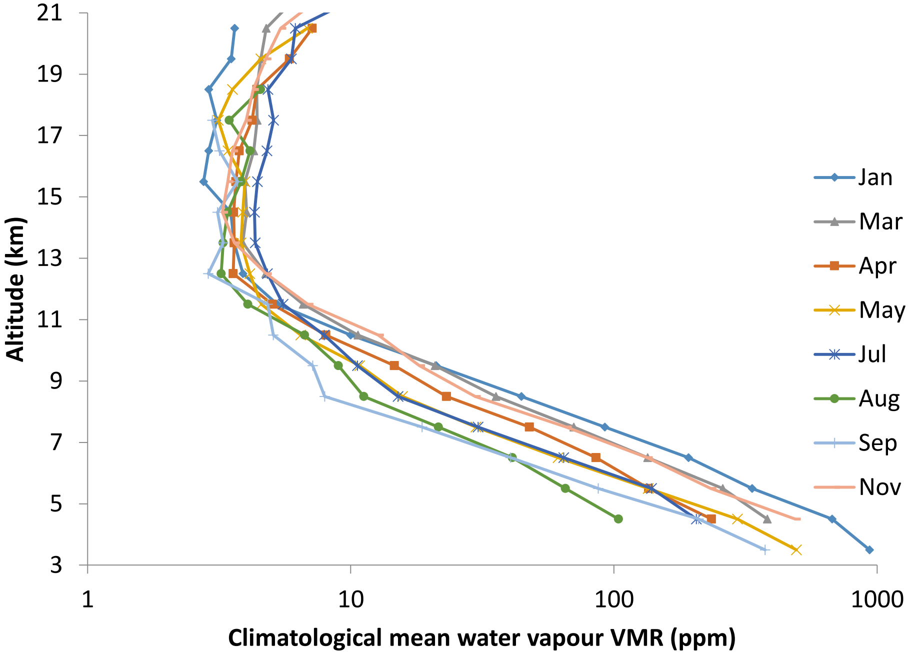

Figure 4. MAESTRO mean climatology (2004–2012) of the vertical distribution of water vapour volume mixing ratio in the Antarctic (60–90° S) UT/LS for months with sufficient sampling of the region. A logarithmic scale is used for the *x* axis.

ACPD
15, 22291–22329, 2015

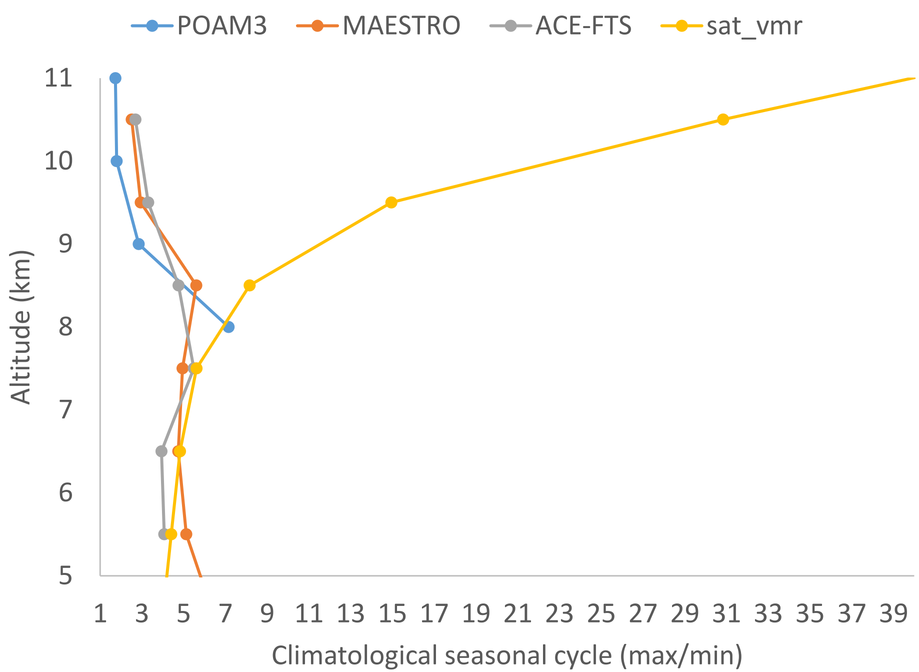

Figure 5. Vertical profile of the seasonal cycle amplitude of Antarctic water vapour observed by three instruments. The amplitude is calculated by taking the ratio of climatological monthly means at maximum (January or December) and minimum (August or September). Note that POAM III has a different orbit that tends to sample consistently at higher latitudes (Nedoluha et al., 2002) and thus tends to have stronger seasonality at 8 km (driven by the larger temperature range). The saturation vapour pressure climatology is obtained using GEM analysis temperatures sampled at ACE measurement locations.

ACPD
15, 22291–22329, 2015

Upper tropospheric water vapour variability at high latitudes – Part 1

C. E. Sioris et al.

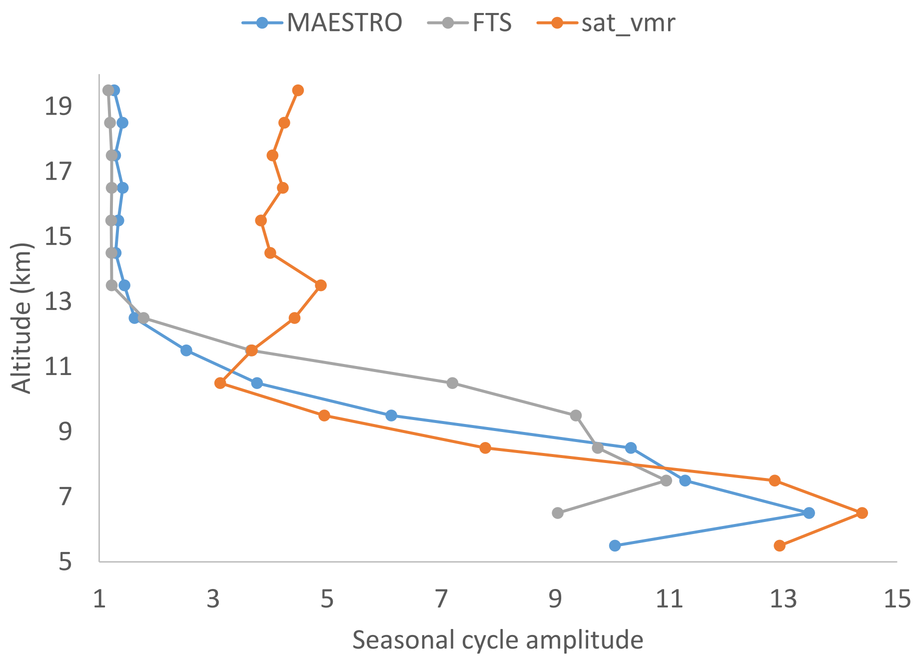

Figure 6. Analogous to Fig. 5 but for northern high latitudes. Profiles are presented at their respective native vertical resolutions.

ACPD
15, 22291–22329, 2015

Upper tropospheric water vapour variability at high latitudes – Part 1

C. E. Sioris et al.

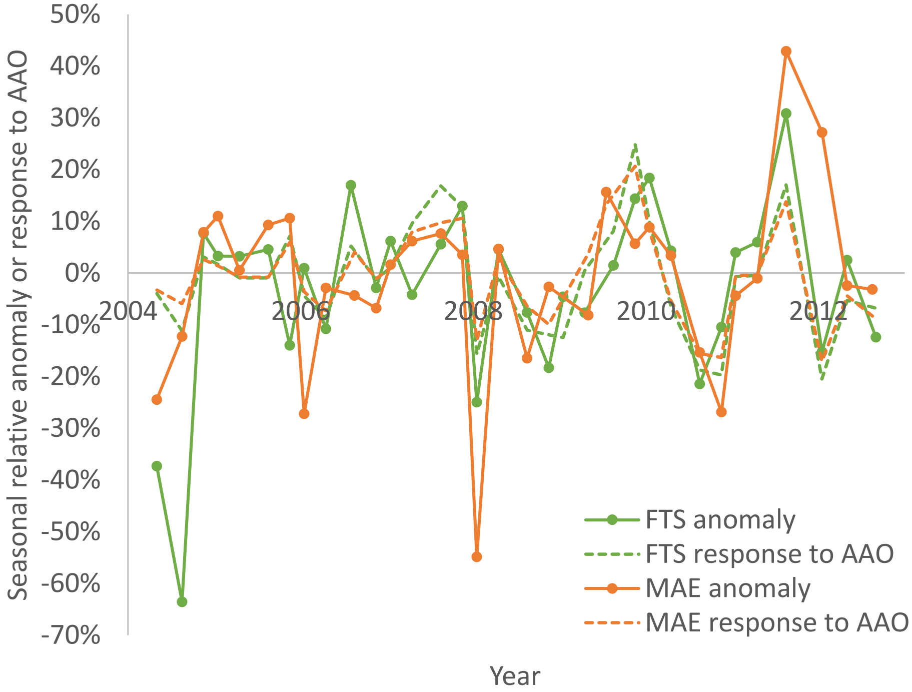

Figure 7. Seasonal median water vapour anomaly time series from MAESTRO (8.5 km) and ACE-FTS (7.5 km) in the Antarctic troposphere and the response of each to AAO determined by linear regression. Seasons with missing data are removed to avoid discontinuities. The markers on the response curves indicate the sampled seasons.

ACPD
15, 22291–22329, 2015

Upper tropospheric water vapour variability at high latitudes – Part 1

C. E. Sioris et al.

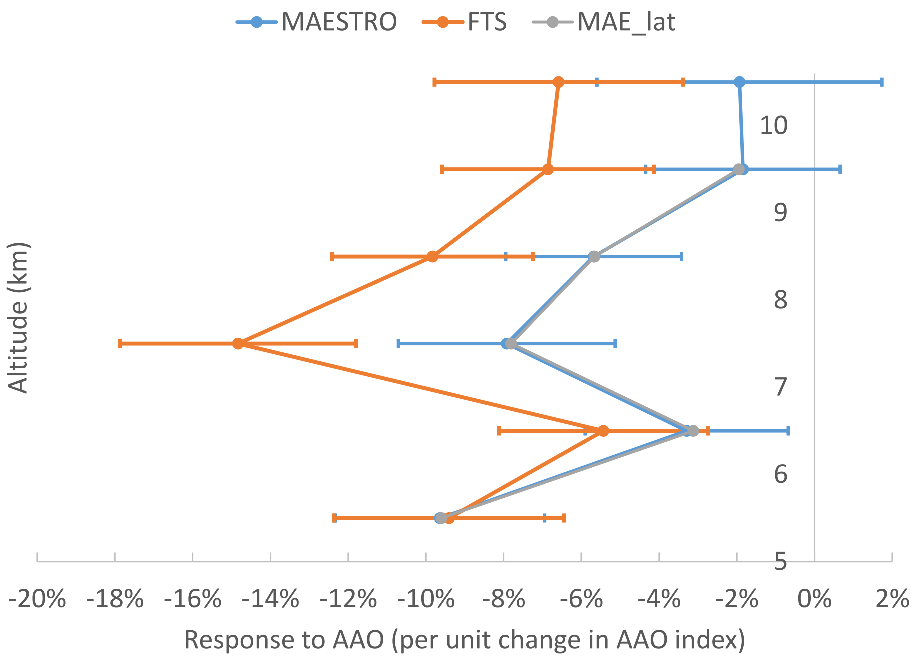

Figure 8. Vertical profile of response to AAO, using southern high latitude water vapour relative anomalies based on monthly medians (2004–2012). Horizontal bars are 1σ standard errors, obtained by linear regression (including a trend term and/or a Puyehue proxy term depending on whether each is significant at the 1σ level). The "MAE_lat" profile shows the MAESTRO water vapour response to AAO upon including a basis function to account for the non-uniform latitudinal sampling.

ACPD
15, 22291–22329, 2015

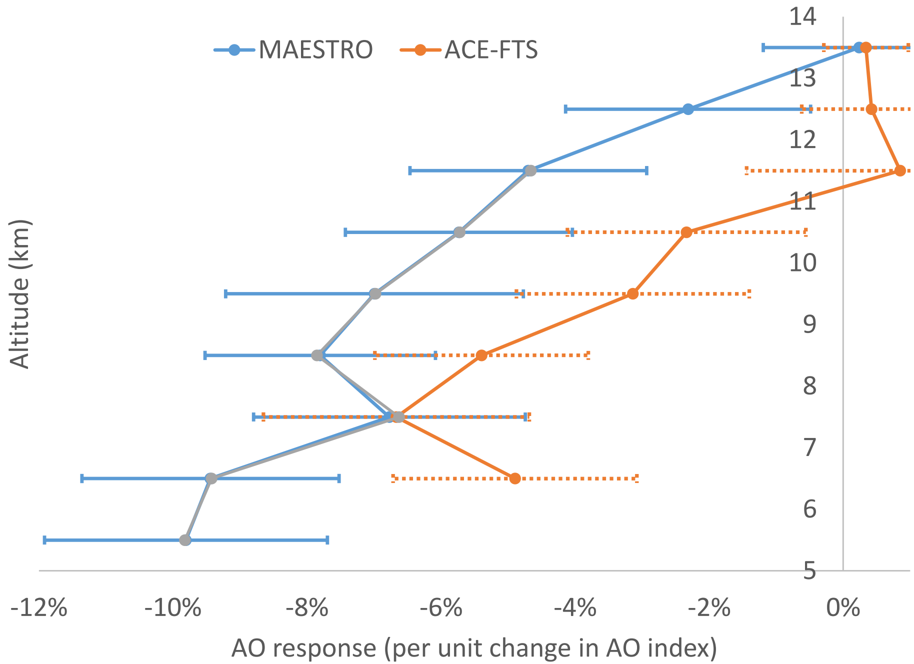

Figure 9. Altitude dependence of northern high-latitude water vapour response to the Arctic oscillation using medians from all available months (analogous to Fig. 8). Error bars display ±1 standard error of the fitting coefficient for the AO index obtained by linear regression.

ACPD
15, 22291–22329, 2015

Upper tropospheric water vapour variability at high latitudes – Part 1

C. E. Sioris et al.

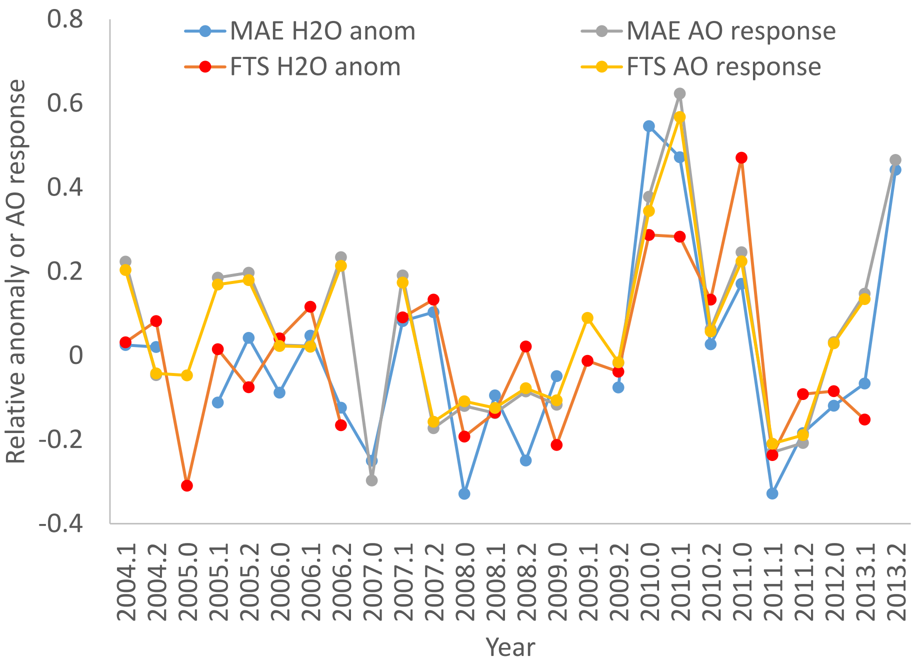

Figure 10. Time series of water vapour relative anomalies observed by ACE-MAESTRO ("MAE") and ACE-FTS at 6.5 ± 0.5 km in winter months (January–March). Slight differences in sampling exist between the two instruments due to the requirement for > 20 observations per month per altitude bin.

ACPD
15, 22291–22329, 2015

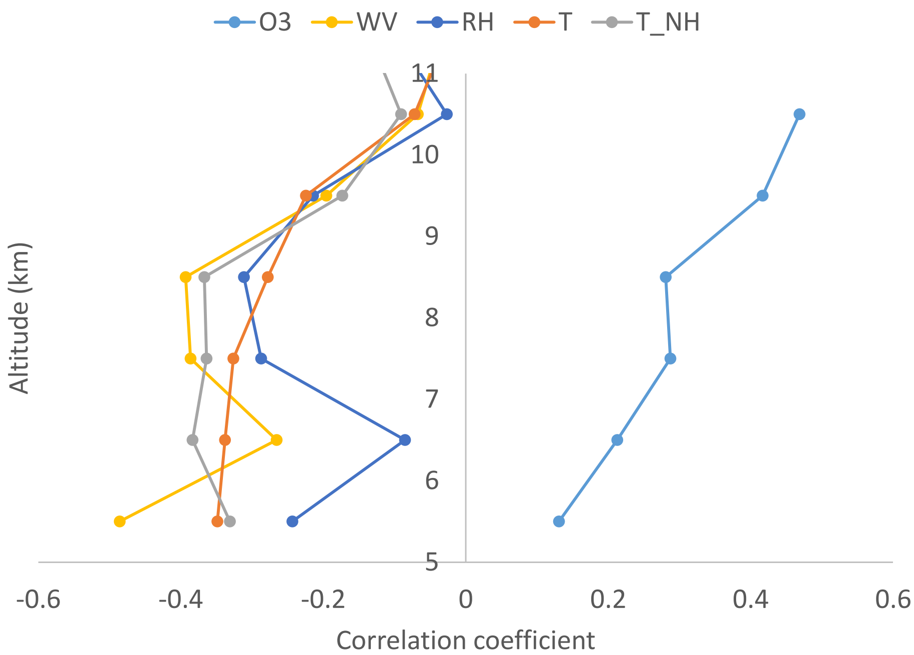

Figure 11. Vertical profile of the correlation between the AAO index and anomalies of several variables at southern high-latitudes in the tropopause region: ACE-FTS ozone, MAESTRO water vapour (WV), RH derived using MAESTRO water vapour, and temperature (T_NH correlates the temperature anomalies in the northern-high latitude region with the AO index to demonstrate the similarity with its southern counterpart).

ACPD
15, 22291–22329, 2015

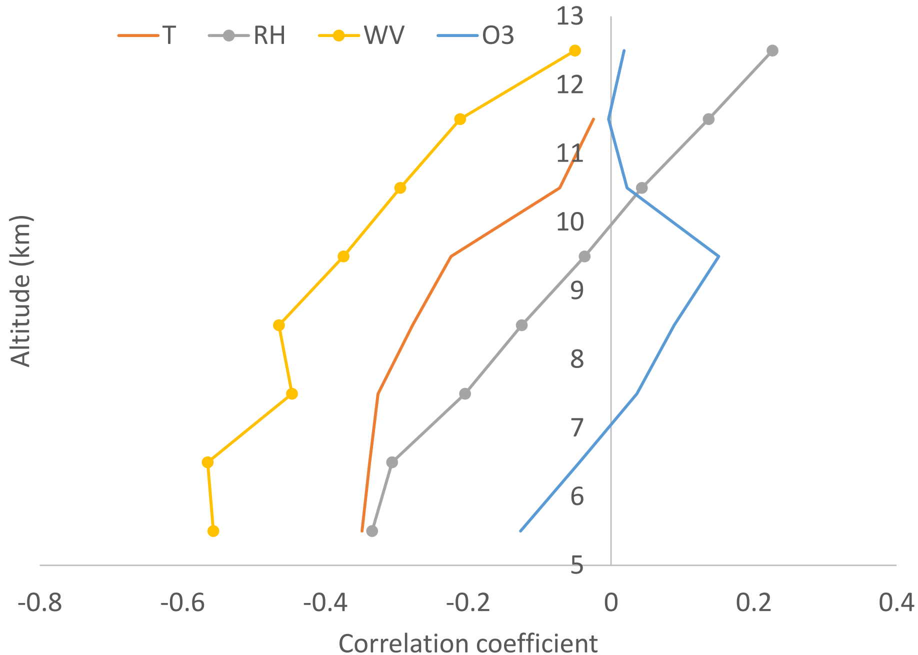

Figure 12. Same as Fig. 11 but for northern high latitudes.

ACPD
15, 22291–22329, 2015

Upper tropospheric water vapour variability at high latitudes – Part 1

C. E. Sioris et al.